Brain Network Reorganization During Visual Search Task Revealed by a Network Analysis of Fixation-Related Potential

Linze Qian, Xianliang Ge, Zhao Feng, Sujie Wang, Jingjia Yuan, Yunxian Pan, Hongqi Shi, Jie Xu, and Yu Sun, *Senior Member, IEEE*

***Abstract*— Visual search is ubiquitous in daily life and has attracted substantial research interest over the past decades. Although accumulating evidence has suggested complex neurocognitive processes underlying visual search, the neural communication across the brain regions remains poorly understood. The present work aimed to fill this gap by investigating functional networks of fixation-related potential (FRP) during the visual search task. Multi-frequency electroencephalogram (EEG) networks were constructed from 70 university students (male/female = 35/35) using FRPs time-locked to target and non-target fixation onsets, which were determined by concurrent eye-tracking data. Then graph theoretical analysis (GTA) and a data-driven classification framework were employed to quantitatively reveal the divergent reorganization between target and non-target FRPs. We found distinct network architectures between target and non-target mainly in the delta and theta bands. More importantly, we achieved a classification accuracy of 92.74% for target and non-target discrimination using both global and nodal network features. In line with the results of GTA, we found that the integration corresponding to target and non-target FRPs significantly differed, while the nodal features contributing most to classification performance primarily resided in the occipital and parietal-temporal areas. Interestingly, we revealed that females exhibited significantly higher local efficiency in delta band when focusing on the search task. In summary, these results provide some of the first quantitative insights into the underlying brain interaction patterns during the visual search process.**

***Index Terms*— EEG, eye-track, fixation-related potential (FRP), functional connectivity, network analysis.**

I. Introduction

HEURISTICALLY, visual perception is the brain's ability to interpret the information received by eyes [1]. It plays an important role in various cognitive functions including reading, writing, and object identification. As one of the key attention mechanisms in the field of visual perception, the top-down pathway combines incoming information with our prior knowledge or expectations, helping to quickly make sense of the environment [2]. Although the top-down modulation on task-related visual perception has already been demonstrated in multiple neuroimaging modalities (i.e., electroencephalogram (EEG) [3], functional magnetic resonance imaging (fMRI) [4], and local field potential (LFP) [5]), existing works investigating the underlying neural mechanisms are inadequate and the current understanding is still rudimentary.

Among neuroimaging techniques, EEG has been widely used due to its low-cost, non-invasiveness, portability, and adaptability to multiple experimental paradigms. To reveal how our brain works during the process of visual perception, traditional event-related potential (ERP) experimental paradigms are typically employed where the participants are requested to identify predetermined stimulus with their eyes fixed to minimize the confounding influence of substantial eye-movements [6]. Nevertheless, it is more often the case in naturalistic scenarios when we actively explore visual scenes to find desired objects through saccades instead of waiting for stimuli appearing on the screen. In this situation, these non-stimulus-locked visual-related events are hard to be identified with uni-modal EEG signal due to complex patterns of eye movements. Actually, eye movements are capable of serving as natural markers corresponding to visual-related events to

Manuscript received 13 September 2022; revised 5 January 2023; accepted 29 January 2023. Date of publication 9 February 2023; date of current version 14 February 2023. This work was supported in part by the National Natural Science Foundation of China under Grant 82172056 and Grant 31800931, in part by the Zhejiang Provincial Natural Science Foundation of China under Grant LR23F010003, in part by the National Key Research and Development Program of China under Grant 2021ZD0200408, in part by the Key Research and Development Program of Zhejiang Province under Grant 2022C03064, in part by the Zhejiang University Global Partnership Fund under Grant 100000-11320, in part by the Science and Technology Special Project of the Institute of Wenzhou, Zhejiang University under Grant XMGL-KJZX-202203, and in part by the Hundred-Talent Program of Zhejiang University. *(Linze Qian and Xianliang Ge contributed equally to this work.) (Corresponding authors: Xianliang Ge; Yu Sun.)*

This work involved human subjects or animals in its research. Approval of all ethical and experimental procedures and protocols was granted by the Institutional Review Board of Zhejiang University.

Linze Qian, Zhao Feng, Sujie Wang, and Jingjia Yuan are with the Key Laboratory for Biomedical Engineering of Ministry of Education of China, Department of Biomedical Engineering, Zhejiang University, Hangzhou, Zhejiang 310027, China.

Xianliang Ge, Yunxian Pan, and Jie Xu are with the Center for Psychological Sciences, Zhejiang University, Hangzhou, Zhejiang 310027, China (e-mail: 0918082@zju.edu.cn).

Hongqi Shi is with the Wuhan Second Ship Design and Research Institute, Wuhan, Hubei 430064, China.

Yu Sun is with the State Key Lab of Brain-Machine Intelligence, Zhejiang University, Hangzhou, Zhejiang 310027, China, also with the Key Laboratory for Biomedical Engineering of Ministry of Education of China, Department of Biomedical Engineering, Zhejiang University, Hangzhou, Zhejiang 310027, China, and also with the Department of Neurology, Sir Run Run Shaw Hospital, Zhejiang University School of Medicine, Hangzhou, Zhejiang 310027, China (e-mail: yusun@zju.edu.cn).

This article has supplementary downloadable material available at https://doi.org/10.1109/TNSRE.2023.3242771, provided by the authors.

Digital Object Identifier 10.1109/TNSRE.2023.3242771

This work is licensed under a Creative Commons Attribution 4.0 License. For more information, see https://creativecommons.org/licenses/by/4.0/

assist active brain-computer interface (BCI) [7]. Considering that uni-modal EEG or eye-tracking signals have already been employed in visual search tasks and have yielded appreciable results [8], [9], several recent efforts have been made to incorporate simultaneous EEG and eye-tracking recording to investigate neural activities under visual perception in the condition of free viewing. In comparison with conventional ERP analysis where EEG is time-locked to external stimulus, EEG can be segmented relative to eye fixations, which is denoted as fixation-related potential (FRP) and has gained substantial interest in various study areas [10], [11], [12].

As a subcategory of ERPs, FRP inherits the characteristic of ERP components and reflects multiple neural activities behind certain fixation events [7]. For instance, lambda response, a positive wave that occurs approximately 80 ms after fixation in occipital areas, is believed to reflect the fundamental visual information process [13]. Moreover, recent investigations have shown it's possible to obtain longer latency FRP components that provide a thorough insight into cognitive mechanisms. Through averaging the EEG signal time-locked to fixations on target object, a relatively late component in FRP associated with P300 potential was observed [14], [15], which is typically related to cognitive functions such as attention and object identification. Considering the ability of P300 in discriminating target stimulus and distractors [16], it can be inferred that the fixation-related P300 could provide discriminative information in terms of FRP classification. For example, Brouwer et al. achieved satisfactory single-trial FRP classification accuracy and revealed the reliable discrimination of a P300-liked FRP component [11]. Similar results were observed in a free viewing experiment where Kaunitz et al. found the great contributions of FRP at around 450 ms to the classification performance [17]. Beyond the fundamental visual information processing within a short post-fixation epoch, these evidences suggest the fixation-related P300 component reflects significant neural activities that could promote FRP classification performance.

Although previous studies successfully distinguished target and non-target fixations using the FRP characteristic in time domain, the relationships among brain regions have been barely explored, which has already shown its promising potential for cognition-related state classification [18]. In fact, our brain is a complex network, within which the information is continuously shared between spatially distributed, but functionally linked brain regions regardless of the brain states [19], [20]. Most recently, network analysis methods have attracted convergent interest and made great achievements in the field of ERP. In recent studies of oddball paradigm, evoked P300 amplitude was found to significantly correlate with the efficiency of resting-state brain network [21] as well as the small-world metrics of functional network in task conditions [22]. In addition, Li et al. revealed the difference in functional brain networks under different stimulus sequences, indicating that the effect of stimulus sequences on P300 network could be quantitatively measured by brain network properties [23]. However, to the best of our knowledge, only one existing work to date has considered network analysis in the field of FRP, which aimed to investigate differences between memory encoding and retrieval processes using an EEG epoch length of 200 ms [24]. The authors revealed that task requirements dynamically control the functional brain network involved in early visual perception. There is still a gap between network analysis and target or non-target FRPs in terms of abundant information in later FRP components.

In our recent work, we have demonstrated that the discriminative FRP features in occipital areas and achieved an appreciable single-trial FRP classification performance [25]. Similar findings have also been reported with regard to saccade-related potential (SRP) where target and non-target SRPs could be distinguished through EEG voltages features [26]. Although satisfactory classification performance was achieved in terms of single-trial FRP or SRP target identification, little attention has been paid in these previous studies to explore the underlying neural mechanisms related to target and non-target identification during the visual search tasks. Motivated by the development of brain network research on ERP, we investigated the differences of underlying network reorganizations between target and non-target FRPs in this work [25]. Specifically, concurrent eye-tracker and EEG signals were recorded during a customized visual search paradigm [27]. To obtain more comprehensive connectivity patterns, EEG was divided into four frequency bands (i.e., delta, theta, alpha, and beta), while a strict artifacts removal process through independent component analysis (ICA) [28] was used to reduce the noise influence. Subsequently, we constructed brain networks using weighted phase lag index (wPLI) [29] and quantitatively assessed the topological network properties. The network metrics were further fed into a machine learning framework synthesized by feature selection and classification processes for FRP identification, while additionally estimating the features' discrimination and investigating their associations with the underlying cognitive processes. Based upon prior neuroimaging research on ERP [22] and FRP [11], [17], [24], we hypothesized that the reorganization of networks differs between target and non-target fixations, which is capable of distinguishing FRPs via several previously-validated classification models. Moreover, on the basis of gender differences in visual perception [30], we further hypothesized that gender would make an impact on the visual search task, which would be shown in both behavioral performance and network metrics.

II. Methods and Materials

A. Participants

In this work, seventy healthy university participants (male/female = 35/35) with a mean age ± standard deviation of 22.4 ± 2.3 years were recruited from Zhejiang University. All participants reported normal or corrected-to-normal vision and were pre-screened through telephone interviews to exclude those with chronic illness, sleep disorder, childhood history of ADHD, or long-term medication history. Prior to the experiment date, they were requested to get sufficient sleep (>7 hours) for 2 consecutive days. Participants consuming caffeine or alcohol, or undertaking strenuous exercise for 24 hours preceding the study were rescheduled. The study protocol was approved by the Institutional Review Board

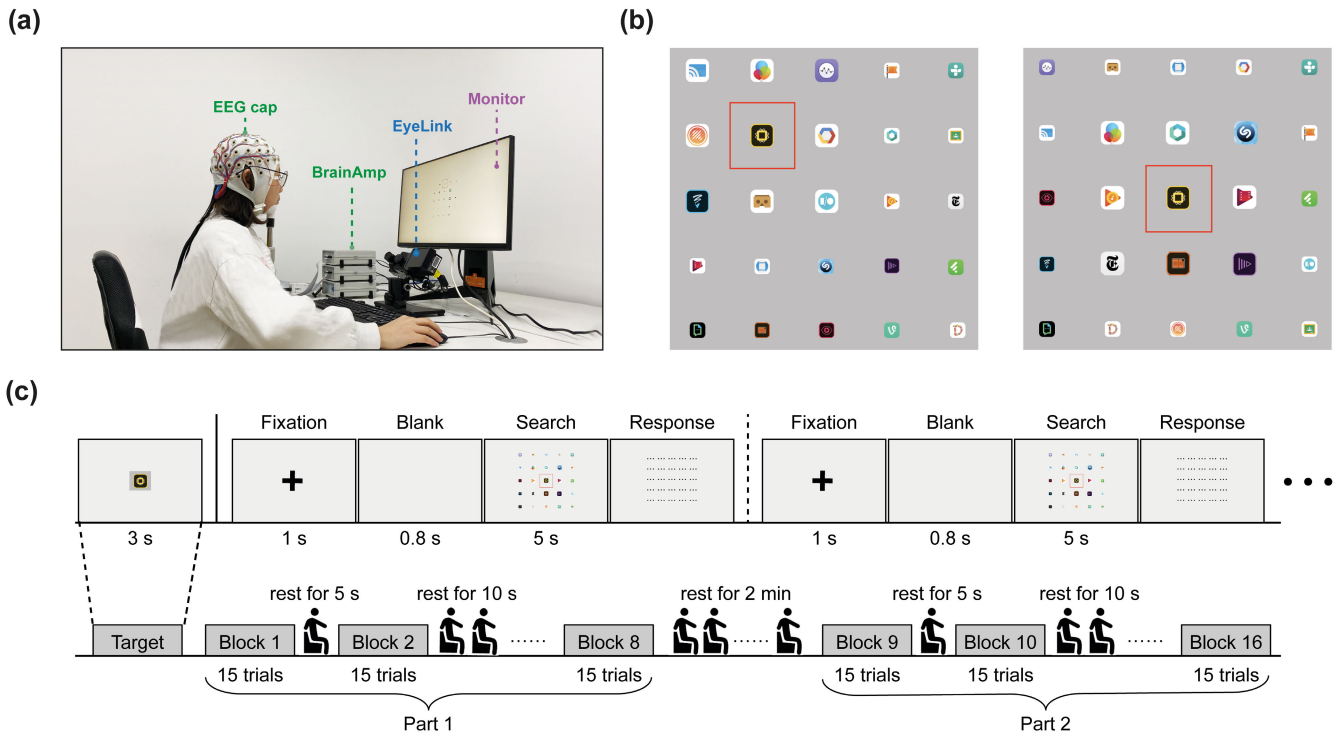

Fig. 1. A schematic diagram of the experiment. (a) Experiment setup for EEG and eye-tracking data collection. (b) Sample screenshots of the searching interface presented on the monitor from two random trials. When the participant gazed upon the AOI (i.e., the red rectangle with a size of 100 × 100 pixels) of a certain icon, the icon was highlighted and enlarged together with the surrounding eight icons for the convenience of identification. (c) Task design for each participant. The experiment consists of two parts with 240 trials in total, where the participants were asked to search for the target icon as quickly and accurately as possible and to memorize its location in search period and confirm the result in response period.

of Zhejiang University and written informed consent was obtained from all participants after the explanation of the experiment.

B. Experimental Design

The details of the experimental paradigm have been described previously in [25] and [27]. Briefly, as illustrated in Fig. 1, the participants were asked to sit in front of the computer screen at a distance of 60 cm (field of view (FOV) = 13.86° × 13.86°) using a chin support. A total of 25 app icons arranged in 5 × 5 were presented on the screen (1920 × 1080 pixels) against a gray background ([R, G, B] = [192, 192, 192]), among which the participants were asked to search for a target icon as quickly and accurately as possible. Initially, the icons were 24 × 24 pixels in size, corresponding to an FOV of 0.67° × 0.67°. During the visual search task, when the gaze was located within a certain icon, the icon and the surrounding eight icons were simultaneously highlighted and 1.5 times enlarged (36 × 36 pixels, FOV = 1° × 1°, Fig. 1(b)).

At the beginning of the experiments, a predefined icon (60 × 60 pixels, FOV = 1.67° × 1.67°) was displayed on the screen for 3-second, indicating the search target in all the following trials. Generally, a trial included the consecutive phases of "Fixation", "Blank", "Search", and "Response" (as shown in Fig. 1(c)). Specifically, each trial started with a fixation cross lasting for 1 s. After a 0.8-second blank screen, the search interface comprising 5 × 5 randomly arranged icons was presented for 5-second, during which the cursor was invisible and the participants were requested to find the target icon and to memorize its location. When finishing the period of search task, the mouse cursor appeared again. Simultaneously, all the icons on the display were masked with a dotted line. At that moment, the participants were required to move the cursor to the position of the target icon and click to confirm the result. Then the program would proceed to the next trial automatically. For each participant, 240 trials were divided into two equal parts, with a 120-second break between them to avoid time-on-task effect. Moreover, a 5-second break and a 10-second break were introduced after completing every 15 trials and 30 trials respectively. To ensure that the participants were familiar with the experimental paradigm, pre-experiment practice was conducted for each participant prior to the real recording. The experiment started after three consecutive blocks with correct responses. Of note, an error rate of 5% (i.e., 240 × 5% = 12 trials) is regarded as the threshold for unsatisfactory performance, and ten additional trials would be added to the experiment for every twelve trials with incorrect responses. For instance, if the participants gave wrong responses in 12 trials out of 240 trials, they were presented with 10 additional trials (i.e., 250 trials in total).

C. Data Acquisition and Preprocessing

In this experiment, eye-tracking and EEG data were collected concurrently. To synchronize two kinds of signals using EyeLink's precise clock, the EyeLink Software Development

Kit (SDK, https://www.sr-support.com/forum-9.html) was utilized to send experimental markers to both the eye-tracking computer and the EEG computer during the search task. The detailed eye-tracking and EEG data acquisition parameters and preprocessing processes are introduced below.

1) Eye-Tracking Data: The EyeLink 1000 Plus eye-tracking system (SR Research, Ottawa, Canada) was adopted to record eye-tracking data at a sampling rate of 1000 Hz, while the software Data Viewer (v4.2.1) was utilized for the data analysis. Prior to the experiment, the eye-tracking system was calibrated for each participant. To identify saccade and fixation events, the software thresholds were set as $8000°\,s^{-2}$ for saccade acceleration and $40°\,s^{-1}$ for saccade velocity. When the current saccade velocity or acceleration exceeds the threshold, the software marked the start of a saccade; otherwise the software marked the end of a saccade. Fixations in the EyeLink system are identified using a saccade-pick algorithm. The software produced a fixation after a saccade end. Moreover, the area of interest (AOI) of an icon was defined as the 100 × 100 pixel area centered on that icon. When the participants gazed upon an AOI of target icon, the fixation was labeled as target, while a fixation was classified as non-target when it fell on an AOI including a non-target icon.

2) EEG Data: EEG data were recorded from 64 Ag/AgCl electrodes arranged according to international 10−20 system with a BrainAmp EEG amplifier (Brain Products, Gilching, Germany). Vertical and horizontal electrooculograms (EOG) were acquired from electrodes placed above and below the right eye (VEOG) and on the lateral to the outer canthi (HEOG) respectively. Electrode impedance was controlled below 10 kΩ throughout the recording and the main interference was avoided by antialiasing with a bandpass (0.5−100 Hz) and a 50 Hz notch filter. Both EEG and EOG were digitized at a sampling rate of 500 Hz using FCz as reference and stored for offline analysis. Among 70 participants, two were ruled out due to data recording issues and another two were excluded through visual inspection for excessive artifacts in the EEG recording. Subsequently, a standard EEG preprocessing pipeline was adopted. Specifically, raw EEG signals were downsampled to 256 Hz and filtered using a 0.5−40 Hz zero-phase FIR bandpass filter. After manual cleaning by visual inspection, ICA was implemented through the extended infomax algorithm [28] to decompose EEG signals into 63 independent components (ICs). ICs with high correlations to EOG signals were removed to correct the ocular artifacts, while muscle activity artifacts related ICs were removed manually (average number of removed ICs: 9.84 ± 3.47, in detail, 9.90 ± 3.34 for males and 9.79 ± 3.64 for females without significant gender difference ($t_{60} = -0.122$, $p = 0.903$)). A common average reference was then applied. All data preprocessing steps were carried out using customized codes and the EEGLAB toolbox [31] in MATLAB R2020a (The MathWorks Inc, US).

D. Epoch Extraction

For FRP analyses, the preprocessed EEG was segmented into epochs time-locked to fixation onset (i.e., the time at which the fixation fell in the AOI), ranging from 200 ms before to 500 ms after fixation onset. Subsequently, an interval from -200 to -100 ms was utilized for baseline correction to prevent the influence of the preceding saccade [12], [14]. According to the results of eye-tracking data analysis introduced in section II-C, FRP epochs were further classified as target epochs and non-target epochs. All the subsequent FRP analyses are conducted on an epoch-level. Of note, a trial might contain multiple target and non-target epochs. To avoid the contamination of signals due to overlapping phenomena, a target would meet the criterion when there existed no non-target fixations or other events (e.g., the end of the search process) 500 ms after it occurred, while a non-target was qualified if there was no target fixation between 500 ms before or after it. In each trial, only the first eligible FRP epochs on the non-target and target that met the criteria mentioned above were considered. Trials corresponding to correct responses were included for epoch extraction and further analyses.

E. Functional Connectivity and Brain Network Construction

To estimate the phase synchronization between each pair of channels, wPLI was utilized to calculate functional connectivity and construct brain networks. As an extension of phase lag index (PLI), wPLI possessed two advantages over PLI in terms of reduced sensitivity to uncorrelated noise and increased ability to capture true changes in phase-synchronization [29]. Briefly, the Hilbert transform was initially employed to obtain the instantaneous phase of signals. Let $x_j(t)$ represent the real-time series of the jth channel; the analytical form $X_j(t)$ is denoted as:

$$X_j(t) = x_j(t) + i\bar{x}_j(t), \tag{1}$$

where $\bar{x}_j(t)$ is the Hilbert transform for $x_j(t)$. If $X_k(t)$ indicates the analytical signal of the k-th channel, the complex cross-spectrum for the two channels can be expressed as:

$$Z(t) = X_j(t)X_k(t)^*, \tag{2}$$

where $X_k(t)^*$ represents the complex conjugate of $X_k(t)$. Then, wPLI is calculated based on the imaginary component of the cross-spectrum:

$$wPLI = \frac{|\langle \Im(Z)\rangle|}{\langle |\Im(Z)|\rangle} = \frac{|\langle |\Im(Z)| sign(\Im(Z))\rangle|}{\langle |\Im(Z)|\rangle}, \tag{3}$$

where $\langle\cdot\rangle$ and $|\cdot|$ refer to mean and absolute value operations respectively, $\Im(Z)$ indicates the imaginary part of Z, and $sign$ denotes the signum function. The value of wPLI ranges from 0 to 1, with 0 indicating no phase consistency between two channels and 1 indicating full synchrony.

Notably, although delta and theta event-related oscillations were regarded as the major contributor to P300 signals [32], accumulating evidence indicated that event-related desynchronization in alpha band was associated and involved in cognitive function such as visual working memory representation [8], while the beta-band oscillations were suggested to be involved in visual processing and attention [33]. With these in mind, the data analysis presented in this study considered four

frequency bands (i.e., delta: 2−4 Hz, theta: 4−8 Hz, alpha: 8−13 Hz, and beta: 13−30 Hz). Specifically, four finite impulse response (FIR) bandpass filters were designed to extract frequency-specific patterns and consequently provide a comprehensive assessment of brain networks. Subsequently, wPLI was calculated in each 500 ms FRP epoch and averaged within two classes (i.e., target and non-target) to amplify the neural connectivity time-locked to the fixation. Consequently, two 63 × 63 weighted matrices corresponding to target and non-target were created for each frequency band and each subject.

F. Network Analysis

First, average connectivity strength was obtained via averaging all the connectivity edges in a network. To remove spurious connections and maintain the most intrinsic connections, a sparsity (i.e., the ratio of the number of existing edges to the maximum possible number of edges in a network) threshold-based approach was adopted prior to the following graph theoretical analysis. By setting the values of those thresholded edges to 1, we constructed binary networks with values of either 0 (unconnected) or 1 (connected) to ensure the assessment of intrinsic between-group differences in the topological structure without bias from different weights of significant connections. Given that no clear definition of an accurate threshold has been provided, a wide range of sparsity thresholds from 0.1 to 0.4 with a step of 0.01 was employed as mentioned in [34]. To avoid multiple comparisons at the individual sparsity threshold and to reduce the dependency of statistical results on the arbitrary choice of a single threshold, integrated metrics (mathematically corresponding to the areas under the metric curve) were estimated for all global and nodal network measures over the predefined sparsity range [34], [35]. Specifically, considering small-world topology, an attractive model for brain organization that is typically characterized as a higher cluster coefficient and a shorter characteristic path length than a random network [36], small-world properties including clustering coefficient (C), characteristic path length (L), and small-worldness (SW) were estimated in this work. To provide a clear and direct physical meaning to the concept of small-world properties from the perspective of information flow [35], global efficiency (E_{global}) and local efficiency (E_{local}) were also calculated. Nodal metrics were estimated using betweenness centrality (BC) and eigenvector centrality (EC). The Brain Connectivity Toolbox (BCT) was employed for the estimation of these graph theoretical metrics [37]. The detailed definitions and descriptions of the above network metrics are presented in the Supplementary Materials.

G. Feature Selection and Classification

To investigate the alterations of the networks properties in various visual search phase from a data-driven modeling perspective, FRP classification was performed with the aforementioned network properties. Using both global (E_{global}, E_{local}, C, L, and SW) and nodal (BC and EC) metrics in four frequency bands, we obtained $5 \times 4 = 20$ global features and $2 \times 63 \times 4 = 504$ nodal features, with the full fusion dataset comprising $20 + 504 = 524$ features for each FRP class and each subject. Then z-score method was applied for feature standardization. To avoid the possible overfitting issue caused by high-dimensional features and obtain reliable and efficient classifiers, we aimed to select an optimal feature subset. To this end, the Fisher score (F-score) was employed to estimate the discriminability of individual features [38], which could be calculated as:

$$F(i) = \frac{\sum_{k=1}^{c} \left(\bar{x}_{k,i} - \bar{x}_i\right)^2}{\sum_{k=1}^{c} \frac{1}{n_k - 1} \sum_{j=1}^{n_k} \left(x_{k,j,i} - \bar{x}_{k,i}\right)^2} \tag{4}$$

where $F(i)$ denotes the F-score of the i-th feature. $\bar{x}_i$ and $\bar{x}_{k,i}$ represent the average of the i-th feature corresponding to the entire dataset and k-th class, respectively. $x_{k,j,i}$ is the value of the i-th feature in the j-th sample of class k. n_k is the number of samples in the k-th class. A larger $F(i)$ value indicates a better discriminability of feature i. Based on the descending sort of all F-score values, a wide range of feature subsets (i.e., from the top 1 to 200) was selected in turn and classified by k-nearest neighbor (KNN). Of note, here the number of neighbors was set as 10, and 10 ten-fold cross-validations were performed in total. Due to the slightly different training set in each fold of cross-validation, the final feature set differed slightly from fold to fold. Thus

Algorithm 1 Classification

Require:
$EEG \in \mathbb{R}^{C \times T}$: raw EEG data;
$labels \in \mathbb{R}^{N_S}$: FRP labels, $labels \in \{0, 1\}$;
Ensure:
Predicted labels corresponding to maximum accuracy;
Set of features with over 50% occurrence rate;
Begin:
1) Constructed functional networks, binarization, calculated integrated global (E_{global}, E_{local}, C, L, and SW) and nodal (BC and EC) metrics;
2) Fully fused network metrics to construct feature set $D \in \mathbb{R}^{N_S \times N_F}$;
for $cv = 1$ to 10 **do** {ten-fold cross-validation}
  D_{test}=D_{cv}
  D_{train}=$D - D_{cv}$
  for $i = 1$ to N_F **do** {feature selection}
    $weights(i) = F\text{-}score(D_{train}, labels)$
  end for
  $rank = sort(weights)$
  for $j = 1$ to 200 **do** {classification (KNN, NB, SVM)}
    $selected = rank(1 : j)$
    $D_{test} = D_{test}^{selected}$
    $D_{train} = D_{train}^{selected}$
    $models = Classifiers(D_{train}^{selected}, labels)$
    $predictions = predict(models, D_{test}^{selected})$
    $acc_{cv,j} = evaluate(predictions, labels)$
  end for
  $acc_j = mean(acc_{cv,j}, 1)$
end for
3) Repeated the above loop for 10 times, calculated the average classification accuracy ave_acc_j;
4) Picked the maximum accuracy across models and feature numbers, obtained corresponding prediction labels and feature number;
5) Calculated the occurrence rate of each feature OR_j, selected features with OR_j greater than 50% as the discriminative feature set.

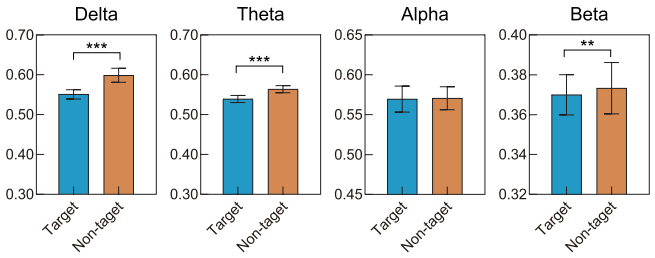

Fig. 2. The statistical differences of average connectivity strength between target and non-target in four frequency bands. Bars represent mean ± standard error. ** represents $p < 0.01$, *** denotes $p < 0.001$.

the contribution of various network metrics to classification performance was not evenly distributed. The occurrence rate was defined as the proportion of network features appearing in the final feature set of each cross-validation fold to a total of 100 (10 × 10) folds. A feature with an occurrence rate over 50% was regarded as a discriminative feature. The classification framework is illustrated in Algorithm II-F. To determine whether the selected features could maintain high classification performance that is independent of different classification models, we performed the classification framework on two additional previously-validated models (i.e., naive Bayesian (NB) and support vector machine (SVM)). Furthermore, to investigate the contribution of various types of features, ten-fold cross-validation was performed based on discriminative feature subsets (i.e., global features, nodal features, and fusion features) obtained from KNN with the aforementioned framework and repeated ten times. In the current work, KNN and NB were implemented based on the Statistics and Machine Learning Toolbox. The number of neighbors was set as 10 for KNN model, while the NB model assumed that the input features were distributed according to Gaussian distribution. The LIBSVM software [39] was employed to build the SVM model, which utilized the radial basis function (RBF) kernel with $\gamma = 0.5$ and the penalty parameter $C = 1$.

H. Statistical Analysis

To investigate the difference in brain states between target and non-target identification, we conducted paired t-test on the average connectivity strength and aforementioned network metrics. Furthermore, we implemented a two-way ANOVA with factor #1 gender (i.e., male and female), factor #2 fixation events (i.e., target and non-target) in this work to explore the gender effect in consideration of network properties. A value of $p < 0.05$ was considered significant. Corrections for multiple comparisons of nodal characteristics were performed via false discovery rate (FDR) correction. The paired t-test was performed using SPSS 26 software (IBM, New York).

To quantitatively assess the significance of classification accuracy, a permutation test was conducted in this work. Briefly, classification was applied 1000 times by randomizing the class labels to estimate the distribution of the classification accuracy. Then p-value was calculated as the probability of the accuracy corresponding to randomized samples to be greater or equal to that in the original samples. Classification performance is considered significant when the p-value is less than 0.05.

III. Result

A. Behavior Performance

Motivation on the task was deemed poor when the accuracy of a participant was 1 S.D. lower than the group average. Consequently, 4 participants were excluded at this step, and the final dataset consisted of 62 participants (male/female = 29/33). On average, the included participants performed well in the visual search task with a mean accuracy of 99.76% (S.D. = 0.41%). Additionally, the Mann-Whitney U test was performed to investigate the gender effect on behavior performance, and no significant difference was found between males and females ($p = 0.524$).

B. Analysis of Global Network Properties

Paired t-test was first adopted to assess the differences in average connectivity strength. Compared with target, significantly higher average connectivity strength for non-target was revealed in delta ($t_{61} = 18.023$, $p < 0.001$), theta ($t_{61} = 17.726$, $p < 0.001$), and beta ($t_{61} = 3.157$, $p = 0.002$) bands (Fig. 2). These results confirmed the necessity of using binary networks for the subsequent network analyses. In Fig. 3, we showed the statistical comparisons of network metrics. Significant differences were mainly found in delta and theta bands for E_{global}, L, and SW. Specifically, non-target showed a higher E_{global} in delta band ($t_{61} = 4.114$, $p < 0.001$) while a lower E_{global} in theta band ($t_{61} = -3.705$, $p < 0.001$) than target. In contrast to E_{global}, L possessed an opposite relationship between two networks; that is, non-target exhibited a lower L in delta band ($t_{61} = -4.141$, $p < 0.001$) while a higher L in theta band ($t_{61} = 3.693$, $p < 0.001$). Moreover, non-target showed significantly lower SW than target in both delta ($t_{61} = -4.123$, $p < 0.001$) and theta ($t_{61} = -4.286$, $p < 0.001$) bands. No significant difference was found in E_{local} and C.

C. Analysis of Nodal Network Properties

To visualize and evaluate nodal properties, the topographical maps of integrated betweenness centrality and eigenvector centrality at each electrode related to target and non-target FRPs were displayed in Fig. 4. Generally, the two nodal properties exhibited similar patterns, and significant differences were mainly found in delta and theta bands, which was in line with the results of global properties. Specifically, all 39 significant BC measures were located in delta (30 measures) and theta (9 measures) bands, while 73 EC measures with significant differences were distributed in delta (37 measures), theta (28 measures), alpha (7 measures) and beta (1 measure) bands. Regarding topological distributions, BC showed an occipital predominance for non-target as well as a parietal-temporal predominance for target in both delta and theta bands, while the same phenomenon in EC was found in delta, theta, and alpha bands.

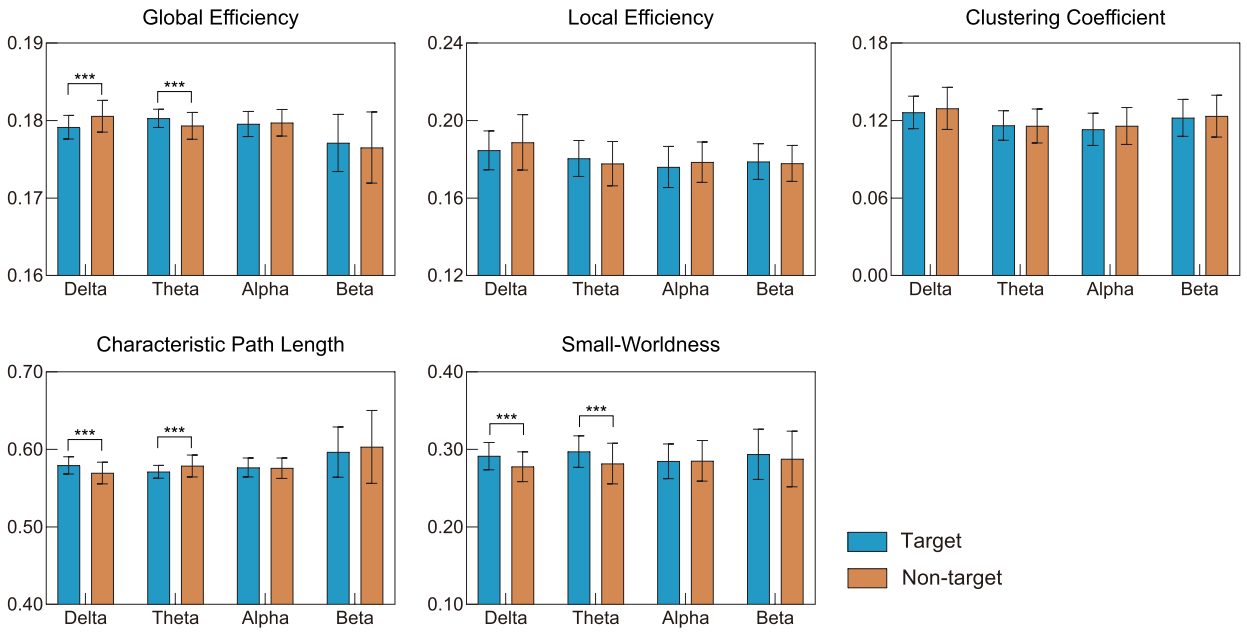

Fig. 3. The statistical differences of global network properties between target and non-target in four frequency bands. Bars represent mean ± standard error. *** denotes $p < 0.001$.

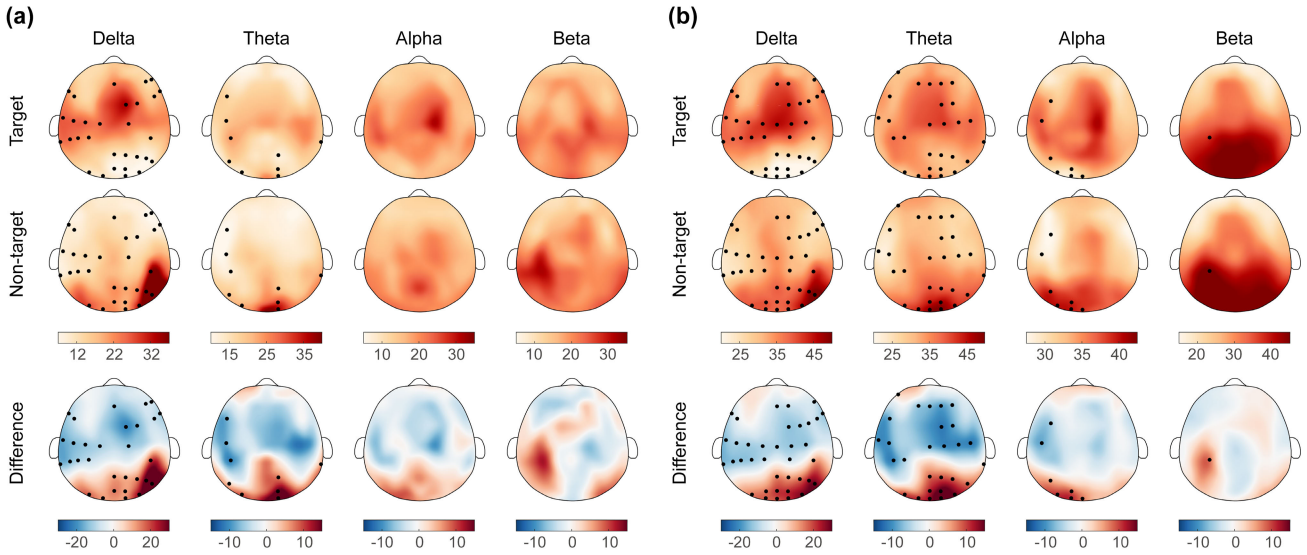

Fig. 4. The topographical maps of integrated (a) betweenness centrality and (b) eigenvector centrality of each node in four frequency bands. Values between electrodes were interpolated in each plot. The unit for eigenvector centrality is 10^{-3}. Difference is defined as non-target minus target under the same conditions. Maps for target and non-target in each frequency band and each metric are presented using the same color scale, while each difference map is proportionally scaled to optimize color contrast. Electrodes highlighted in black represent the corresponding measures with p-values lower than 0.05 after FDR correction.

D. Classification Performance and Discriminative Features

FRP classification was performed to explore the divergent network properties. The receiving operator characteristic (ROC) curve of each classifier corresponding to the highest accuracy across feature numbers is shown in Fig. 5(a). As presented, all three classifiers (i.e., KNN, NB, and SVM) achieved satisfactory classification performance. Among the three classifiers, the best classification performance was achieved by KNN with an accuracy of 92.74% ($p < 0.001$, 1000 permutations, sensitivity = 93.06%, specificity = 92.42%, Fig. 5(b)) and an area under the ROC curve (AUC) of 0.971 when utilizing 87 selected features. Under this circumstance, we then investigated the discriminative features based on their occurrence rate. As such, 85 out of 524 features exceeded the predefined threshold, of which 6 were global and 79 were nodal. Specifically, global network features included E_{global}, L, and SW in delta and theta bands, while nodal network features primarily resided in occipital, and parietal-temporal areas. The detailed descriptions of discriminative nodal features are shown in Fig. 5(c). Moreover, the classification results based on discriminative features showed satisfactory performance significantly above the chance level for all feature

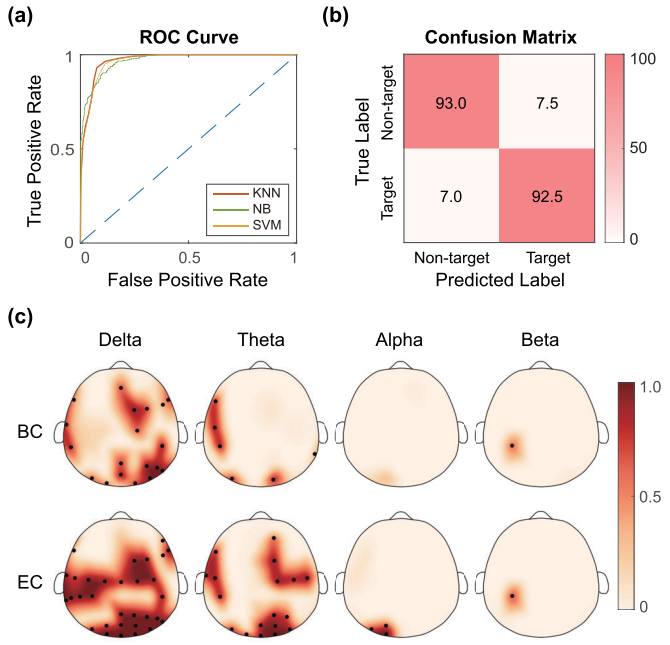

Fig. 5. The results of FRP classification. (a) ROC curves for KNN, NB, and SVM under the best accuracy across feature numbers. The dotted line in blue represents random guess. (b) Confusion matrix for KNN. (c) The topological maps of occurrence rate calculated according to optimal classification performance of KNN. Electrodes highlighted in black represent the corresponding measures with occurrence rates greater than 50%.

TABLE I
CLASSIFICATION RESULTS BASED ON DISCRIMINATIVE FEATURES

	Global Features	Nodal Features	Fusion Features
Accuracy	76.21% ***	93.79% ***	94.44% ***
AUC	0.814 ***	0.980 ***	0.983 ***

Note: *** denotes $p < 0.001$, 1000 permutations.

subsets (Table I). The highest performance was obtained with an accuracy of 94.44% and an AUC of 0.983 (for both metrics, $p < 0.001$, 1000 permutations) when using 85 fusion features, while a comparable performance was achieved with 79 nodal features (accuracy = 93.79%, AUC = 0.980, $p < 0.001$), and a much poorer performance was obtained with 6 global features (accuracy = 76.21%, AUC = 0.814, $p < 0.001$).

E. Gender Effect

To investigate the gender effect on visual search tasks, the two-way ANOVA was adopted to examine the network properties between male and female under different fixation events. Interestingly, the E_{local} in delta band showed significant interaction effect ($F_{1,120} = 4.369$, $p = 0.039$), but no significant main effect was found (gender: $F_{1,120} = 2.685$, $p = 0.104$, task: $F_{1,120} = 3.031$, $p = 0.084$). Further post-hoc tests revealed that the significant interaction effect was attributed to the higher delta E_{local} of non-target in females compared with that of target in females ($F_{1,120} = 7.845$, $p = 0.006$) and that of non-target in males ($F_{1,120} = 6.952$, $p = 0.009$).

IV. DISCUSSION

To the best of our knowledge, this is the first study performing network analysis methodology on long-term FRPs to investigate the differences between target and non-target identification in a visual search task. The significant findings are as follows: first, divergent reorganizations of brain network were revealed between target and non-target FRPs during the visual search at both global and local levels. Second, we distinguished target and non-target FRPs with satisfactory accuracy based on the proposed classification framework. Further exploration of discriminative features showed the key role of delta and theta frequency bands, while the topographical distribution of nodal metrics revealed the predominance of occipital and parietal-temporal areas. Third, further investigation found an interaction effect in delta band local efficiency between genders and fixation events, with females exhibiting higher value than males in the process of search. The findings were mostly consistent with the hypotheses that both fixation events and gender would lead to different brain reorganization patterns and would be discussed in greater detail below.

A. FRP Classification Performance

To investigate the network reorganization from the perspective of a data-driven modeling approach, FRP classification was performed. The ROC curves in Fig. 5(a) showed comparable performance with above 0.9 AUC for all three classifiers, revealing the generality of the proposed framework. Through KNN, we obtained the highest classification accuracy of 92.74% and the AUC of 0.971 with 87 features employed. Paired to the very low p-value of the permutation test, the excellent performance indicated the effectiveness of the adopted classification framework along with network properties for target and non-target FRPs discrimination. Additionally, we also assessed the performance of the proposed classification framework using all 524 features and the main results were largely consistent with that using 200 features (detailed results were shown in Supplementary Materials), indicating the weak relevance of the rest features to the classification results. Further interrogations of the contributing features indicated that the performance was primarily attributed to nodal features rather than global features, which might be due to the limited number of global features. Moreover, the incorporation of nodal features together with global features enhanced the performance of KNN. Actually, distinguishing target and non-target identification events using FRP is not a trivial problem, as FRP is typically contaminated by successive eye movements [40]. Compared with other studies examining FRP classifications [11], [17], [25], our classification framework achieved the highest accuracy. The optimal classification performance might be attributed to the following two points. First, considering that EEG recognition is a challenging task due to its low signal-to-noise ratio (SNR) characteristic, here we improved the SNR via averaging target and non-target FRP epochs respectively for each participant, while the aforementioned studies performed single-trial FRP classification. This concept was also supported by Pfeiffer et al., who observed improvements in FRP decoding performance from single-trial to 40-trial averages [41]. Second, as FRP generally manifests as temporal variations in EEG amplitude time-locked to fixation onsets, time point features

(i.e., the concatenation of EEG samples from certain or all channels) have typically been used for classification in previous studies [11], [17], [25], [42]. However, the contribution of time point features to classification performance is relatively limited, emphasizing the need to explore more discriminative FRP characteristics [25]. Considering the significantly divergent network patterns revealed in this work, the optimal classification performance might partially be due to more discriminative network features, which is in line with the concept that functional networks can provide additional information and help better characterize brain states [43]. Moreover, it's noteworthy that we performed classification on the whole dataset consisting of data from different individuals, suggesting the potential of network-based features for cross-subject FRP classification, which is of particular importance for future practical applications.

B. FRP Related Network Biomarker

FRPs related to target and non-target tend to reflect different cognitive processes [7], and the corresponding neural biomarkers could be suggested by discriminative network properties. Here, we explored the discriminative features based on their occurrence rate. In line with the statistical results, we found that the network metrics with high occurrence rates almost exhibited significant differences. In accordance with findings of important delta-theta activities in P300 components analysis (for a review, see [32]), our results showed that the discriminative features at both the global and nodal levels were primarily located in delta and theta bands.

1) Global Network Biomarker: Prior to the topological network properties, the investigation of connectivity edges revealed the significantly higher average connectivity strength in delta, theta, and beta bands for non-target, suggesting the more closely linked brain areas and increased information processing efficiency [21]. Heuristically, brain network patterns corresponding to different frequency bands are assumed to play a crucial role during the cognitive process [44]. Specifically, delta oscillations were found to be linked to cognition-related attention [45], while theta activities were associated with successful memory retrieval [46]. In visual attention tasks, the ventral visual pathway from the primary visual cortex to the inferior temporal cortex is typically active [47], [48], thus leading to increased global integration [49]. Considering that non-target FRP involved both brain response to standard stimuli and attention on subsequent searching process, we further indicated that the brain may recruit more resources to facilitate parallel information transfer efficiency and maintain focused during the search process, consequently manifesting as higher delta global efficiency in non-target. As target FRP implied the brain response to deviant stimuli and memorization processes, the higher theta global efficiency in target could be explained by the long-range theta phase synchronization for target processing [46]. Similar findings have also been reported in a visual search work in which increased theta fronto-parietal connectivity was observed during anticipation of a specific visual target [50]. In terms of characteristic path length, it's inversely related to global efficiency, thus showing comparable occurrence rates and significances in both bands. In particular, recent evidence has shown small-world brain network patterns in several cognitive tasks [36]. Further explorations revealed a relationship between delta-theta connectivity and working memory [51], while memory encoding exhibited significantly higher small-worldness than storage or retrieval [52]. Therefore, we speculated that the findings of higher delta and theta small-worldness in target were mainly due to cognitive functions such as encoding and storing the coordinates of the target.

2) Nodal Network Biomarker: Nodes with a high centrality were more likely to play an important role in brain networks, and our findings indicated a similar distribution of the adopted two metrics. Specifically, nodes with high centrality were primarily located in occipital area for non-target and parietal area for target. Our findings therefore provided additional evidence to support the notion that occipital regions are crucial for visual attention and top-down control [53], while parietal areas are associated with memory processing [54]. In addition, the different distributions in frontal-parietal regions were also probably due to differences between fovea-related and periphery-related processes in visual cognition [55], implying a greater cognitive demand for target identification [56]. Despite similar characteristics, the two centrality properties still reflected various aspects of cognitive function. Theoretically, nodes with high betweenness centrality tend to facilitate the information exchange along the most efficient path, consequently leading to more integrated networks [57]. Hence, we suggested that the evidently higher delta betweenness centrality in occipital-temporal areas (PO8, P6, P8, and CP6) for non-target was related to underlying ventral visual pathways [47], promoting the integration of the brain network. Regarding eigenvector centrality, it determines the relative importance of regions within the whole-brain network hierarchy, which can provide additional information compared with betweenness centrality [58]. The enhanced alpha eigenvector centrality nodes in occipital regions for non-target might be associated with the guidance of visual perception that integrates sensory evidence with task demands [59].

C. Gender Effect on FRP Network Properties

Though there was no significant difference in behavioral performance between genders, the present study revealed a significant gender difference in the underlying organization of brain networks. In recent years, a considerable amount of literature had been published suggesting structural and functional differences in the brain between genders [60], [61], [62]. For example, in [60], a stronger association between gray matter volume and cognitive performance was revealed in females using magnetic resonance imaging (MRI). And Tomasi et al. indicated that women exhibited a higher brain connectivity strength that may optimize cognitive functions requiring integration [62]. These findings suggested that gender might have a great impact on P300-related cognitive tasks [63]. Partially in agreement with previous researches indicating females showed a greater local efficiency than males using diffusion magnetic resonance imaging (dMRI) [64], fMRI [65], and EEG [66] in the resting-state, we extended

the results to the task-related condition with similar findings, indicating a higher allocation of attention resources in females during visual search. It might owe to a more elaborated event-categorization process accompanied by a more distinct sensory input in females [67].

D. Methodology Considerations

There still existed some factors that needed to be considered when interpreting the results of the current study. Though a study conducted by Bahar et al. have confirmed the reliability to explore connectivity patterns in source space through EEG source localization methods [68], we merely constructed functional connectivity networks in sensor space using a feasible method to reduce the influence of volume conduction. Nonetheless, the relationship between brain regions in cortical space could be ulteriorly investigated in future studies to assess the reproducibility of the main findings. Moreover, prior work has already compared brain response to target and standard stimuli recorded in an experiment with eye fixed [69]. However, in this work, EEG epochs corresponding to non-target might be significantly distorted by eye movements and overlapping brain responses related to saccades [40]. It would provide specific phase relationship patterns and subsequently influence the network connectivity based on phase synchronization [40]. In fact, approaches like ICA or other linear models might not consider the full variety of factors accounting for the overlapping and fail to remedy this problem. Therefore, in order to extract clean EEG data corresponding to target and non-target information processes and investigate their differences in visual search situations, new experiment protocols [70] or signal processing algorithms [71] were encouraged for further validation of current findings.

V. Conclusion

In this study, we explored, for the first time, the brain networks constructed by long-term FRPs related to target and non-target identification in the visual search experiment. Specifically, through graph theoretical analysis and a data-driven modeling approach, we revealed FRP related neural biomarkers at both the global and nodal levels, indicating the divergent network reorganization patterns during the visual search task. Moreover, satisfactory classification performance was achieved through utilizing the fusion of both global and nodal network features, suggesting its potential to improve the FRP decoding accuracy. Furthermore, we observed a significant gender difference in terms of delta local efficiency, highlighting the potential gender influence in further visual search-related studies. In summary, our findings provide the first quantitative evidence to show the underlying brain interaction patterns and facilitate the understanding of neural mechanisms during the visual search process.

References

[1] J. Yang, C. Wang, B. Jiang, H. Song, and Q. Meng, "Visual perception enabled industry intelligence: State of the art, challenges and prospects," *IEEE Trans. Ind. Informat.*, vol. 17, no. 3, pp. 2204–2219, Mar. 2021.

[2] J. Theeuwes, "Visual selection: Usually fast and automatic; seldom slow and volitional," *J. Cognition*, vol. 1, no. 1, p. 21, May 2018.

[3] P. J. Matusz, N. Turoman, R. I. Tivadar, C. Retsa, and M. M. Murray, "Brain and cognitive mechanisms of top–down attentional control in a multisensory world: Benefits of electrical neuroimaging," *J. Cognit. Neurosci.*, vol. 31, no. 3, pp. 412–430, Mar. 2019.

[4] M. S. Spetter et al., "Neural correlates of top-down guidance of attention to food: An fMRI study," *Physiol. Behav.*, vol. 225, Oct. 2020, Art. no. 113085.

[5] N. Ramalingam, J. N. J. Mcmanus, W. Li, and C. D. Gilbert, "Top-down modulation of lateral interactions in visual cortex," *J. Neurosci.*, vol. 33, no. 5, pp. 1773–1789, Jan. 2013.

[6] C. Wang, J. Xu, S. Zhao, and W. Lou, "Graph theoretical analysis of EEG effective connectivity in vascular dementia patients during a visual oddball task," *Clin. Neurophysiol.*, vol. 127, no. 1, pp. 324–334, Jan. 2016.

[7] D. Wobrock, A. Finke, T. Schack, and H. Ritter, "Using fixation-related potentials for inspecting natural interactions," *Frontiers Hum. Neurosci.*, vol. 14, p. 447, Nov. 2020.

[8] I. E. J. de Vries, J. van Driel, and C. N. L. Olivers, "Posterior α EEG dynamics dissociate current from future goals in working memory-guided visual search," *J. Neurosci.*, vol. 37, no. 6, pp. 1591–1603, Feb. 2017.

[9] I. Jeelani, A. Albert, K. Han, and R. Azevedo, "Are visual search patterns predictive of hazard recognition performance? Empirical investigation using eye-tracking technology," *J. Construct. Eng. Manage.*, vol. 145, no. 1, Jan. 2019, Art. no. 04018115.

[10] F. Degno and S. P. Liversedge, "Eye movements and fixation-related potentials in reading: A review," *Vision*, vol. 4, no. 1, p. 11, Feb. 2020.

[11] A.-M. Brouwer, B. Reuderink, J. Vincent, M. A. J. van Gerven, and J. B. F. van Erp, "Distinguishing between target and nontarget fixations in a visual search task using fixation-related potentials," *J. Vis.*, vol. 13, no. 3, p. 17, Feb. 2013.

[12] H. Hiebel, A. Ischebeck, C. Brunner, A. R. Nikolaev, M. Höfler, and C. Körner, "Target probability modulates fixation-related potentials in visual search," *Biol. Psychol.*, vol. 138, pp. 199–210, Oct. 2018.

[13] A. J. Ries, D. Slayback, and J. Touryan, "The fixation-related lambda response: Effects of saccade magnitude, spatial frequency, and ocular artifact removal," *Int. J. Psychophysiology*, vol. 134, pp. 1–8, Dec. 2018.

[14] H. Devillez, N. Guyader, and A. Guérin-Dugué, "An eye fixation–related potentials analysis of the P300 potential for fixations onto a target object when exploring natural scenes," *J. Vis.*, vol. 15, no. 13, p. 20, Sep. 2015.

[15] A. Frey, G. Ionescu, B. Lemaire, F. López-Orozco, T. Baccino, and A. Guérin-Dugué, "Decision-making in information seeking on texts: An eye-fixation-related potentials investigation," *Frontiers Syst. Neurosci.*, vol. 7, p. 39, Aug. 2013.

[16] H. Wang et al., "Performance enhancement of P300 detection by multiscale-CNN," *IEEE Trans. Instrum. Meas.*, vol. 70, pp. 1–12, 2021.

[17] L. N. Kaunitz, J. E. Kamienkowski, A. Varatharajah, M. Sigman, R. Q. Quiroga, and M. J. Ison, "Looking for a face in the crowd: Fixation-related potentials in an eye-movement visual search task," *NeuroImage*, vol. 89, pp. 297–305, Apr. 2014.

[18] I. Kakkos et al., "EEG fingerprints of task-independent mental workload discrimination," *IEEE J. Biomed. Health Informat.*, vol. 25, no. 10, pp. 3824–3833, Oct. 2021.

[19] F. Taya, Y. Sun, F. Babiloni, N. Thakor, and A. Bezerianos, "Brain enhancement through cognitive training: A new insight from brain connectome," *Frontiers Syst. Neurosci.*, vol. 9, p. 44, Apr. 2015.

[20] D. S. Bassett and O. Sporns, "Network neuroscience," *Nature Neurosci.*, vol. 20, no. 3, pp. 353–364, Feb. 2017.

[21] F. Li et al., "Relationships between the resting-state network and the P3: Evidence from a scalp EEG study," *Sci. Rep.*, vol. 5, p. 15129, Oct. 2015.

[22] F. Li et al., "The construction of large-scale cortical networks for P300 from scalp EEG," *IEEE Access*, vol. 6, pp. 68498–68506, 2018.

[23] F. Li et al., "Different contexts in the oddball paradigm induce distinct brain networks in generating the P300," *Frontiers Hum. Neurosci.*, vol. 12, p. 520, Jan. 2019.

[24] H. Seidkhani, A. R. Nikolaev, R. N. Meghanathan, H. Pezeshk, A. Masoudi-Nejad, and C. van Leeuwen, "Task modulates functional connectivity networks in free viewing behavior," *NeuroImage*, vol. 159, pp. 289–301, Oct. 2017.

[25] X. Ge et al., "Improving intention detection in single-trial classification through fusion of EEG and eye-tracker data," *IEEE Trans. Human-Mach. Syst.*, vol. 53, no. 1, pp. 132–141, 2023.

[26] A.-M. Brouwer, M. A. Hogervorst, B. Oudejans, A. J. Ries, and J. Touryan, "EEG and eye tracking signatures of target encoding during structured visual search," *Frontiers Hum. Neurosci.*, vol. 11, p. 264, May 2017.

[27] Y. Pan, X. Ge, L. Ge, and J. Xu, "Using eye-controlled highlighting techniques to support both serial and parallel processing in visual search," *Appl. Ergonom.*, vol. 97, Nov. 2021, Art. no. 103522.

[28] T.-W. Lee, M. Girolami, and T. J. Sejnowski, "Independent component analysis using an extended infomax algorithm for mixed subgaussian and supergaussian sources," *Neural Comput.*, vol. 11, no. 2, pp. 417–441,1999.

[29] M. Vinck, R. Oostenveld, M. Van Wingerden, F. Battaglia, and C. M. A. Pennartz, "An improved index of phase-synchronization for electrophysiological data in the presence of volume-conduction, noise and sample-size bias," *NeuroImage*, vol. 55, no. 4, pp. 1548–1565, Apr. 2011.

[30] M. C. W. English, M. T. Maybery, and T. A. W. Visser, "Magnitude of sex differences in visual search varies with target eccentricity," *Psychonomic Bull. Rev.*, vol. 28, no. 1, pp. 178–188, Sep. 2020.

[31] A. Delorme and S. Makeig, "EEGLAB: An open source toolbox for analysis of single-trial EEG dynamics including independent component analysis," *J. Neurosci. Methods*, vol. 134, no. 1, pp. 9–21, Mar. 2004.

[32] C. Başar-Eroglu, E. Başar, T. Demiralp, and M. Schürmann, "P300-response: Possible psychophysiological correlates in delta and theta frequency channels. A review," *Int. J. Psychophysiol.*, vol. 13, no. 2, pp. 161–179, 1992.

[33] M. C. McCusker, A. I. Wiesman, M. D. Schantell, J. A. Eastman, and T. W. Wilson, "Multi-spectral oscillatory dynamics serving directed and divided attention," *NeuroImage*, vol. 217, Aug. 2020, Art. no. 116927.

[34] J. Li et al., "Mid-task break improves global integration of functional connectivity in lower alpha band," *Frontiers Hum. Neurosci.*, vol. 10, p. 304, Jun. 2016.

[35] S. Achard and E. Bullmore, "Efficiency and cost of economical brain functional networks," *PLoS Comput. Biol.*, vol. 3, no. 2, p. e17, Feb. 2007.

[36] D. S. Bassett and E. D. Bullmore, "Small-world brain networks," *Neuroscientist*, vol. 12, no. 6, pp. 512–523, 2007.

[37] M. Rubinov and O. Sporns, "Complex network measures of brain connectivity: Uses and interpretations," *NeuroImage*, vol. 52, no. 3, pp. 1059–1069, 2010.

[38] P. Li et al., "EEG based emotion recognition by combining functional connectivity network and local activations," *IEEE Trans. Biomed. Eng.*, vol. 66, no. 10, pp. 2869–2881, Oct. 2019.

[39] C. C. Chang and C. J. Lin, "LIBSVM: A library for support vector machines," *ACM Trans. Intell. Syst. Technol.*, vol. 2, no. 3, pp. 1–27, 2011.

[40] A. R. Nikolaev, R. N. Meghanathan, and C. van Leeuwen, "Combining EEG and eye movement recording in free viewing: Pitfalls and possibilities," *Brain Cogn.*, vol. 107, pp. 55–83, Aug. 2016.

[41] C. Pfeiffer, N. Hollenstein, C. Zhang, and N. Langer, "Neural dynamics of sentiment processing during naturalistic sentence reading," *NeuroImage*, vol. 218, Sep. 2020, Art. no. 116934.

[42] F. Lotte et al., "A review of classification algorithms for EEG-based brain–computer interfaces: A 10 year update," *J. Neural Eng.*, vol. 15, no. 3, Apr. 2018, Art. no. 031005.

[43] V. Gonuguntla, Y. Wang, and K. C. Veluvolu, "Event-related functional network identification: Application to EEG classification," *IEEE J. Sel. Topics Signal Process.*, vol. 10, no. 7, pp. 1284–1294, Oct. 2016.

[44] Y. Xi, Q. Li, M. Zhang, L. Liu, and J. Wu, "Characterizing the time-varying brain networks of audiovisual integration across frequency bands," *Cognit. Comput.*, vol. 12, no. 6, pp. 1154–1169, Nov. 2020.

[45] G. G. Knyazev, "EEG delta oscillations as a correlate of basic homeostatic and motivational processes," *Neurosci. Biobehavioral Rev.*, vol. 36, no. 1, pp. 677–695, Jan. 2012.

[46] G. T. Waldhauser, K.-H.-T. Bäuml, and S. Hanslmayr, "Brain oscillations mediate successful suppression of unwanted memories," *Cerebral Cortex*, vol. 25, no. 11, pp. 4180–4190, Nov. 2015.

[47] G. A. Rousselet, S. J. Thorpe, and M. Fabre-Thorpe, "How parallel is visual processing in the ventral pathway?" *Trends Cogn. Sci.*, vol. 8, no. 8, pp. 363–370, Aug. 2004.

[48] M. Eimer, "The neural basis of attentional control in visual search," *Trends Cogn. Sci.*, vol. 18, no. 10, pp. 526–535, Oct. 2014.

[49] B. Parhizi, M. R. Daliri, and M. Behroozi, "Decoding the different states of visual attention using functional and effective connectivity features in fMRI data," *Cogn. Neurodyn.*, vol. 12, no. 2, pp. 157–170, Apr. 2018.

[50] A. L. Biel, T. Minarik, and P. Sauseng, "EEG cross-frequency phase synchronization as an index of memory matching in visual search," *NeuroImage*, vol. 235, Jul. 2021, Art. no. 117971.

[51] E. L. Johnson, D. King-Stephens, P. B. Weber, K. D. Laxer, J. J. Lin, and R. T. Knight, "Spectral imprints of working memory for everyday associations in the frontoparietal network," *Frontiers Syst. Neurosci.*, vol. 12, p. 65, Jan. 2019.

[52] J. Toppi et al., "Different topological properties of EEG-derived networks describe working memory phases as revealed by graph theoretical analysis," *Frontiers Hum. Neurosci.*, vol. 11, p. 637, Jan. 2018.

[53] D. Veniero, J. Gross, S. Morand, F. Duecker, A. T. Sack, and G. Thut, "Top-down control of visual cortex by the frontal eye fields through oscillatory realignment," *Nature Commun.*, vol. 12, no. 1, pp. 1–13, Mar. 2021.

[54] A. W. Gilmore, S. E. Kalinowski, S. C. Milleville, S. J. Gotts, and A. Martin, "Identifying task-general effects of stimulus familiarity in the parietal memory network," *Neuropsychologia*, vol. 124, pp. 31–43, Feb. 2019.

[55] R. W. Lefco, J. A. Brissenden, A. L. Noyce, S. M. Tobyne, and D. C. Somers, "Gradients of functional organization in posterior parietal cortex revealed by visual attention, visual short-term memory, and intrinsic functional connectivity," *NeuroImage*, vol. 219, Oct. 2020, Art. no. 117029.

[56] J. O. Maximo, A. Neupane, N. Saxena, R. M. Joseph, and R. K. Kana, "Task-dependent changes in frontal–parietal activation and connectivity during visual search," *Brain Connectivity*, vol. 6, no. 4, pp. 335–344, May 2016.

[57] C. J. Stam, P. Tewarie, E. Van Dellen, E. C. W. van Straaten, A. Hillebrand, and P. Van Mieghem, "The trees and the forest: Characterization of complex brain networks with minimum spanning trees," *Int. J. Psychophysiology*, vol. 92, no. 3, pp. 129–138, Jun. 2014.

[58] K. E. Joyce, P. J. Laurienti, J. H. Burdette, and S. Hayasaka, "A new measure of centrality for brain networks," *PLoS ONE*, vol. 5, no. 8, Aug. 2010, Art. no. e12200.

[59] R. F. Helfrich, M. Huang, G. Wilson, and R. T. Knight, "Prefrontal cortex modulates posterior alpha oscillations during top-down guided visual perception," *Proc. Nat. Acad. Sci. USA*, vol. 114, no. 35, pp. 9457–9462, Aug. 2017.

[60] R. C. Gur et al., "Sex differences in brain gray and white matter in healthy young adults: Correlations with cognitive performance," *J. Neurosci.*, vol. 19, no. 10, pp. 4065–4072, May 1999.

[61] G. Gong, Y. He, and A. C. Evans, "Brain connectivity: Gender makes a difference," *Neuroscientist*, vol. 17, no. 5, pp. 575–591, Oct. 2011.

[62] D. Tomasi and N. D. Volkow, "Gender differences in brain functional connectivity density," *Hum. Brain Mapping*, vol. 33, no. 4, pp. 849–860, Apr. 2012.

[63] S. Melynyte, G. Y. Wang, and I. Griskova-Bulanova, "Gender effects on auditory P300: A systematic review," *Int. J. Psychophysiology*, vol. 133, pp. 55–65, Nov. 2018.

[64] G. Gong, P. Rosa-Neto, F. Carbonell, Z. J. Chen, Y. He, and A. C. Evans, "Age- and gender-related differences in the cortical anatomical network," *J. Neurosci.*, vol. 29, no. 50, pp. 15684–15693, Dec. 2009.

[65] L. Tian, J. Wang, C. Yan, and Y. He, "Hemisphere- and gender-related differences in small-world brain networks: A resting-state functional MRI study," *NeuroImage*, vol. 54, no. 1, pp. 191–202, Jan. 2011.

[66] M. Jalili, "EEG-based functional brain networks: Hemispheric differences in males and females," *Netw. Heterogeneous Media*, vol. 10, no. 1, pp. 223–232, Feb. 2015.

[67] N. Jaušovec and K. Jaušovec, "Gender related differences in visual and auditory processing of verbal and figural tasks," *Brain Res.*, vol. 1300, pp. 135–145, Nov. 2009.

[68] B. Moezzi and M. R. Goldsworthy, "Commentary: Consistency of EEG source localization and connectivity estimates," *Frontiers Neurosci.*, vol. 12, pp. 590–601, Mar. 2018.

[69] F. Li et al., "The time-varying networks in P300: A task-evoked EEG study," *IEEE Trans. Neural Syst. Rehabil. Eng.*, vol. 24, no. 7, pp. 725–733, Jul. 2016.

[70] N. Bigdely-Shamlo, A. Vankov, R. R. Ramirez, and S. Makeig, "Brain activity-based image classification from rapid serial visual presentation," *IEEE Trans. Neural Syst. Rehabil. Eng.*, vol. 16, no. 5, pp. 432–441, Oct. 2008.

[71] A. Tremblay and A. J. Newman, "Modeling nonlinear relationships in ERP data using mixed-effects regression with R examples," *Psychophysiology*, vol. 52, no. 1, pp. 124–139, Jan. 2015.